

Ytterbium-driven strong enhancement of electron-phonon coupling in graphene

Choongyu Hwang^{1,2}, Duck Young Kim³, D. A. Siegel^{1,4}, Kevin T. Chan^{1,4}, J. Noffsinger^{1,4}, A. V. Fedorov⁵, Marvin L. Cohen^{1,4}, Börje Johansson⁶, J. B. Neaton^{4,7,8}, and A. Lanzara^{1,4*}

¹*Materials Sciences Division, Lawrence Berkeley National Laboratory, Berkeley, CA 94720, USA*

²*Department of Physics, Pusan National University, Busan 609-735, Republic of Korea*

³*Geophysical Laboratory, Carnegie Institution of Washington, Washington DC 20015, USA*

⁴*Department of Physics, University of California, Berkeley, CA 94720, USA*

⁵*Advanced Light Source, Lawrence Berkeley National Laboratory, Berkeley, CA 94720, USA*

⁶*Department of Materials and Engineering, Royal Institute of Technology, Stockholm, SE-100 44, Sweden*

⁷*The Molecular Foundry, Lawrence Berkeley National Laboratory, Berkeley, CA 94720, USA and*

⁸*Kavli Energy Nanosciences Institute at Berkeley, Berkeley, CA 94720, USA.*

(Dated: October 9, 2018)

We present high-resolution angle-resolved photoemission spectroscopy study in conjunction with first principles calculations to investigate how the interaction of electrons with phonons in graphene is modified by the presence of Yb. We find that the transferred charges from Yb to the graphene layer hybridize with the graphene π bands, leading to a strong enhancement of the electron-phonon interaction. Specifically, the electron-phonon coupling constant is increased by as much as a factor of 10 upon the introduction of Yb with respect to as grown graphene (≤ 0.05). The observed coupling constant constitutes the highest value ever measured for graphene and suggests that the hybridization between graphene and the adatoms might be a critical parameter in realizing superconducting graphene.

PACS numbers: 71.38.-k, 72.10.Di, 73.20.-r, 79.60.-i

I. INTRODUCTION

The interaction of electrons with phonons is of practical and fundamental interest in graphene, as it not only affects the transport properties of actual devices [1], but also induces novel phenomena such as charge density waves [2] and superconductivity [3]. Hence the manipulation of the electron-phonon coupling is an important issue to realize graphene-based electronic and spintronic devices [4] and to create new strongly correlated electron phases. In fact, several methods have been proposed to modify the electron-phonon coupling constant, λ , of graphene using charge carrier density [5], magnetic field [6], disorder [7], and adatoms [8]. Among them, the change of charge carrier density can tune the strength of electron-phonon coupling up to $\lambda \leq 0.05$ [5], while electron-electron interactions are efficiently suppressed [9]. On the other hand, the presence of adatoms is predicted to drastically enhance electron-phonon coupling up to $\lambda = 0.61$ [8], so that graphene enters the regime where phonon-mediated superconductivity might exist [8, 10]. However, experimental evidence of this striking enhancement in graphene has been controversial so far.

The most prominent manifestation of the electron-phonon coupling is a renormalization or kink of the electronic band structure at the phonon energy accompanied by a change in the charge carrier scattering rate. These effects are directly observed using angle-resolved photoemission spectroscopy (ARPES) [11]. However, experi-

mental studies on the role of adatoms for the electron-phonon coupling of graphene via ARPES have been debated due to the hybridization of the adatom band with the graphene π bands, referred to as band structure effect, resulting in an apparent enhancement and anisotropy of the electron-phonon coupling strength [12–14]. On the other hand, strong enhancement of the electron-phonon coupling through adatom intercalation have been reported for graphite, and discussed in same cases as the driver for superconductivity [15, 16]. These previous results suggest the importance of combining experimental and theoretical studies to understand the enhancement of electron-phonon coupling in graphene.

Here we present high-resolution ARPES study showing a strong enhancement of the electron-phonon coupling strength in a monolayer graphene sheet via Yb adsorption. A direct comparison with the theoretical band structure determined by first principles calculations show that the Yb 6s electrons transferred to the graphene layer are hybridized with the graphene π bands, resulting in an enhanced electron-phonon coupling from $\lambda = 0.05$ for as grown graphene to $\lambda = 0.43$ for graphene with Yb. This observation constitutes the highest value ever measured for graphene and is in line with the density-functional perturbation theory that predicts an enhancement of λ from 0.02 to 0.51.

* ALanzara@lbl.gov

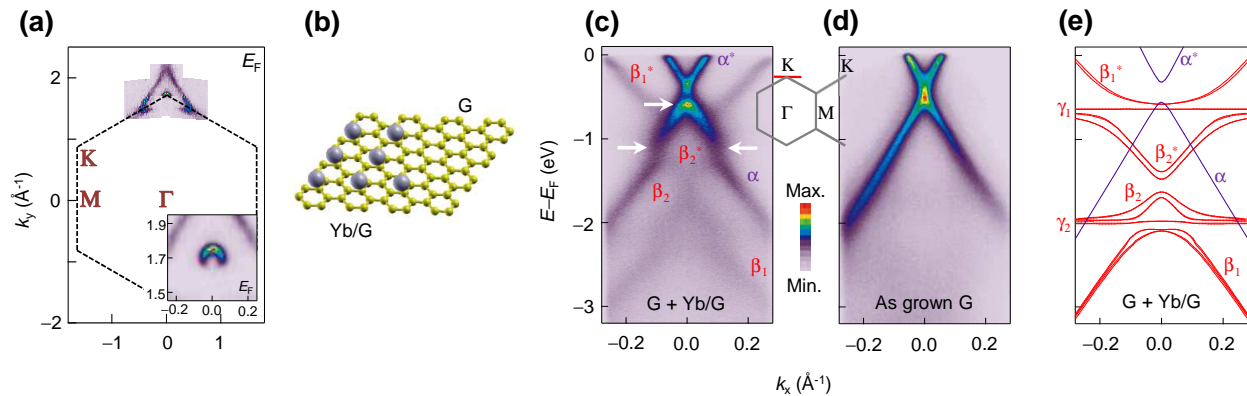


FIG. 1. (Color online) (a) Fermi surface of graphene upon the introduction of Yb. Inset shows a zoomed-in view near the K point (k_x, k_y)=(0, 1.7). (b) Schematic drawing of crystal structure of graphene with inhomogeneous contribution of Yb (the buffer layer and the SiC substrate are not drawn for simplicity). (c-d) Raw ARPES data of graphene in the presence of Yb (G+Yb/G: panel (c)) and as grown graphene (As grown G: panel (d)), through the K point perpendicular to the Γ K direction as denoted by the red line in the inset. (e) Calculated bands of graphene in the presence of Yb (G+Yb/G) perpendicular to the Γ K direction. The G and Yb/G bands are purple and red curves, respectively. The graphene π bands are denoted by α and α^* , and the Yb/G π bands by β and β^* . Yb $4f_{7/2}$ and $4f_{5/2}$ electrons are denoted by γ_1 and γ_2 .

II. METHODS

A. Experimental details

Single layer graphene was grown epitaxially on a 6H-SiC(0001) substrate by an e-beam heating method as described elsewhere [17]. Yb was deposited on graphene at 100 K, followed by repeated annealing processes from 400 K to 1000 K to find a stable geometric structure. This process is well-known to enhance intercalation of alkali- and alkali-earth metals such as K and Ca [12], Rb and Cs [18]. This is also true for Yb [19, 20] when annealed above ~ 200 °C. As a result, the graphene sample in the presence of Yb exhibits a coexisting phase of Yb-intercalated graphene and graphene without Yb, as observed in Fig. 1(a). High-resolution ARPES experiments were performed at beamline 12.0.1 of the Advanced Light Source in ultra-high vacuum maintained below 2×10^{-11} Torr using a photon energy of 50 eV. The energy and angular resolutions were 32 meV and $\leq 0.2^\circ$, respectively. The measurement temperature was 15 K.

B. Electronic band structure calculations

The electronic band structure of graphene with Yb are obtained for YbC₆ by *ab initio* total energy calculations with a plane-wave basis set [21] performed using the Vienna Ab-initio Simulation Package (VASP) [22–24]. Projector augmented wave (PAW) potentials [25, 26] with a plane-wave cutoff of 500 eV are used. The exchange-correlation of electrons was treated within the generalized gradient approximation (GGA) as implemented by Perdew, Burke, and Ernzerhof [27]. The comparison between the measured and the calculated bands using

GGA+U correction to the f electrons of Yb bears 2.0 eV for the on-site Coulomb interaction (U) and 0.7 eV for the intra-atomic exchange interaction (J) [28]. These values differ from 5.4 eV and 0.7 eV, respectively, expected for Yb-intercalated graphite as extracted from the full potential linear augmented plane wave method (LAPW) with $LDA+U$ correction [29]. The U value calculated within $LDA+U$ scheme is usually an overestimate due to the confined screening charge in the same atomic sphere [29]. Although it is not straightforward to directly compare U values estimated by two different correction methods, Yb/G shows smaller value than that of Yb-intercalated graphite.

III. RESULTS

Figure 1(a) shows a photoelectron intensity map at E_F as a function of two dimensional wave vectors k_x and k_y , for graphene with Yb. Two pieces of Fermi surface can be clearly distinguished: one with a crescent-like shape centered at the Brillouin zone corner K (zoomed-in in the inset), which resembles the one measured for as grown graphene on SiC(0001) [30], and the other with a triangular shape with the apex near the M point, similar to that of highly electron-doped graphene [12]. The observation of these two Fermi surfaces suggests a coexistence of graphene with and without Yb, as schematically shown in Fig. 1(b), similar to the case of Rb- and Cs-adsorbed graphene [18] and consistent with previous results on Yb-intercalated graphene [19, 20]. An estimate of the charge doping in the graphene π bands introduced by Yb is given by the area enclosed by the Fermi surface. The occupied area for the crescent-like Fermi surface is 0.025 \AA^{-2} , which corresponds to an electron doping of

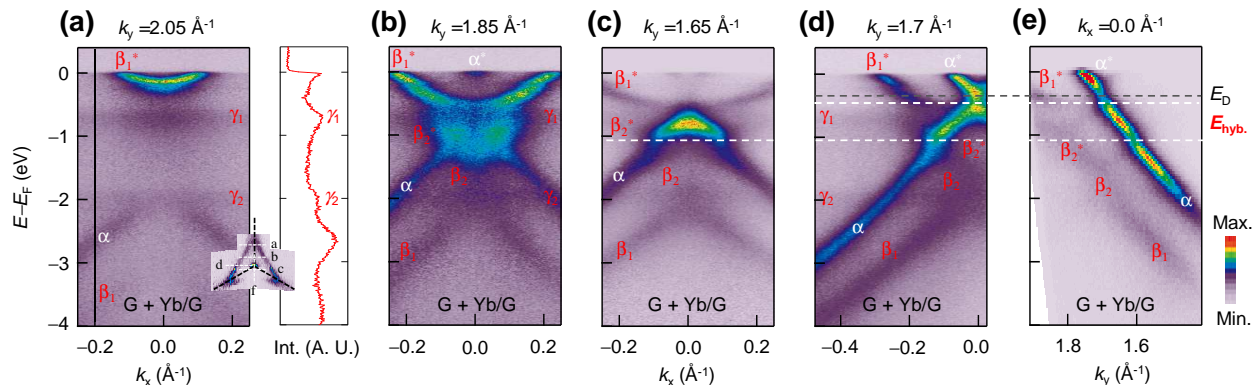


FIG. 2. (Color online) (a) Energy spectra of the Yb/G band taken perpendicular to the Γ K direction at $k_y=2.05 \text{ \AA}^{-1}$ denoted in the inset. The intensity spectrum is taken at $k_x=-0.2 \text{ \AA}^{-1}$ denoted by the black solid line. (b-d) Energy spectra of the Yb/G band taken perpendicular to the Γ K direction at $k_y=1.85, 1.65,$ and 1.7 \AA^{-1} , respectively, denoted in the inset of panel (a). (e) Energy spectra of the Yb/G bands parallel to the Γ K direction denoted in the inset of panel (a). E_{hyb} represents the hybridization energy between the G (α) and Yb/G (β_2^* and β_1^*) bands, denoted by white dashed lines, and E_D is the Dirac energy.

$n \sim 1.2 \times 10^{13} \text{ cm}^{-2}$, similar to the one reported for as grown graphene [31]. The larger triangular Fermi surface, which corresponds to an area of 0.33 \AA^{-2} , yields a much higher electron doping of $n \sim 1.7 \times 10^{14} \text{ cm}^{-2}$. The electronic band structure of the former crosses E_F at $k_x = \pm 0.063 \text{ \AA}^{-1}$ (spectra with the strongest intensity in Fig. 1(c)) with a Dirac point at $\sim -0.4 \text{ eV}$, which resembles as grown graphene shown in Fig. 1(d), except for the observed discontinuities around 0.6 eV and 1.1 eV below E_F as denoted by white arrows in Fig. 1(c). On the other hand, the electronic band structure of the latter crosses E_F at $k_x = \pm 0.26 \text{ \AA}^{-1}$ (spectra with the weakest intensity in Fig. 1(c)) with a Dirac point at $\sim -1.6 \text{ eV}$.

Figure 1(e) shows the calculated electronic band structure for the inhomogeneous sample, where closed packed islands of YbC₆ (referred to as “Yb/G” bands) coexist with islands of clean graphene without Yb (referred to as “G” bands). The G bands, shown in purple and denoted by α and α^* , are the well known graphene π bands obtained within the tight-binding formalism [32] in the presence of an energy gap of 0.2 eV at E_D [33, 34], while the origin of the gap-like feature is still controversial [34–38]. The Yb/G bands, shown in red and obtained by *ab initio* pseudopotential total energy calculations with a plane-wave basis set [21], are denoted by $\beta_1, \beta_1^*, \beta_2, \beta_2^*, \gamma_1,$ and γ_2 . β and β^* are the π bands of the Yb/G, while γ_1 and γ_2 are the Yb $4f_{7/2}$ and $4f_{5/2}$ electrons, respectively. The Yb $4f$ electrons are strongly hybridized with β^* and β bands at 0.7 eV and 2.0 eV below E_F , respectively, resulting in a departure of the Yb/G band from β^* to β_1^* and β_2^* , and from β to β_1 and β_2 . The observed discontinuities at the crossing points of α with β_1^* and β_2^* (white arrows in Fig. 1(c)) may indicate that the G and Yb/G are electronically coupled with each other.

The γ_1 and γ_2 bands show weak spectral intensity with respect to the other bands near the K point. Their rel-

ative intensity is enhanced away from the K point, as shown in Figs. 2(a-d), in which ARPES data were taken perpendicular to the Γ K direction at several k_y values denoted in the inset of Fig. 2(a). The position of γ_1 and γ_2 is determined by the intensity spectrum at $k_x = -0.2 \text{ \AA}^{-1}$ denoted by a black solid line in Fig. 2(a). The hybridization between the Yb/G and Yb bands is clear at $k_y = 1.85 \text{ \AA}^{-1}$ as shown in Fig. 2(b). The deformation of the Yb/G band from β^* to β_1^* and β_2^* is observed at the crossing points with the γ_1 band. The β band also shows unusual discontinuity at the crossing points with the γ_2 band as shown in Figs. 2(b) and 2(c). Such a hybridization is not observed between the G band and Yb $4f$ electrons, e.g., α does not show such a deformation or discontinuity at the crossing point with the γ_2 band around $(E - E_F, k_x) = (-2.0, -0.26)$ in Fig. 2(d). On the other hand, the hybridization between the Yb/G and G bands is clear from the energy spectra not only along k_x direction (Figs. 2(c) and Fig. 2(d)), but also along k_y direction (Fig. 2(e)). At $k_y = 1.65 \text{ \AA}^{-1}$ and $k_y = 1.7 \text{ \AA}^{-1}$ (Figs. 2(c) and 2(d)), discontinuities of the G band are observed at the crossing points with the Yb/G (β_2^* and β_1^*) bands around -1.1 eV below E_F . At $k_x = 0.0 \text{ \AA}^{-1}$ (Fig. 2(e)), weak spectral intensity of the G band is observed at the crossing points with the Yb/G bands around -0.5 eV and -1.1 eV below E_F denoted by E_{hyb} with white dashed lines.

IV. DISCUSSIONS

The calculated electronic band structure provides another important information on the Yb/G system, i.e., the π bands of the Yb/G crossing E_F (β_1^*) exhibits non-zero contribution from Yb $6s$ electrons in addition to the heavy carbon π character. In order to understand

the impact of this hybridization on the electronic properties, we investigate energy spectra measured near E_F in comparison to calculated bands. Figures 3(a) and 3(b) are raw ARPES data of as grown graphene and Yb/G samples, respectively, along the direction denoted by the red line in the inset of each panel. To compare the measured and calculated bands quantitatively, we extract energy-momentum dispersions using the standard method, i. e., Lorentzian fit to the momentum distribution curves (MDCs). The measured band of as grown graphene is well described by the tight-binding band, the black curve in Figs. 3(a) and 3(c). On the other hand, the measured Yb/G band (β_1^*) shows a clear kinked structure around 0.16 eV below E_F as denoted by an arrow in Fig. 3(d), which is not expected in the GGA+U band, the purple curve in Figs. 3(b) and 3(d). A similar structure, although much weaker, is also observed in the G bands (arrows in Fig. 3(c)). Such a kinked structure has been extensively studied in the literature in the context of band renormalization due to the interaction of electrons with phonons [39–43].

Before proceeding to a direct comparison between the effect of such renormalization on G and Yb/G, and the consequent extraction of the electron-phonon coupling constant, it is imperative to establish whether these low energy kinked structures are real manifestation of many body physics or just reflect the bare band structure of this doped sample. Figure 4 shows a comparison of the near

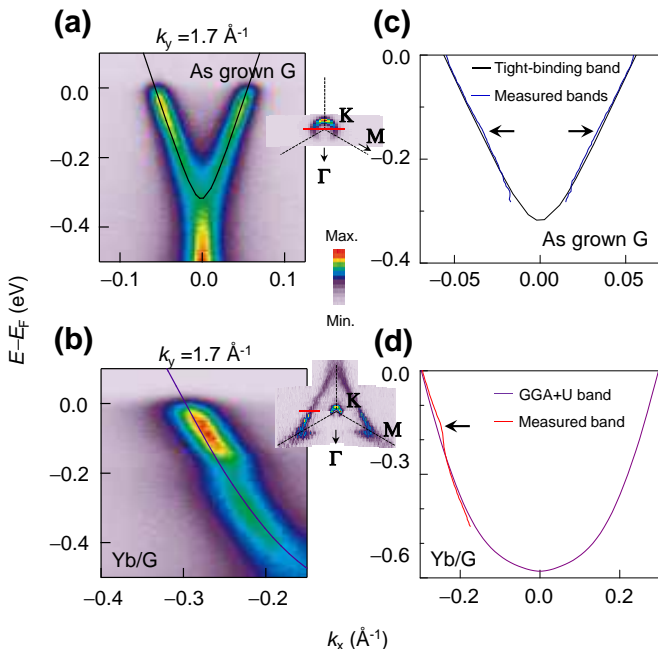


FIG. 3. (Color online) (a-b) Raw ARPES data for the as grown G (panel (a)) and Yb/G (β_1^* : panel (b)) samples near E_F along the direction denoted by the red line in the inset. (c-d) Comparison of measured and calculated bands of as grown G (panel (c)) and Yb/G (panel (d)). The deviation at low energy in the range of 0.2 eV from E_F is denoted by arrows.

E_F band structure for Yb/G along the two directions (KM: panel (a) and KK: panel (b)) with the GGA+U bands. Along the KM direction (Fig. 4(a)), the measured band structure clearly shows a kinked structure around 0.16 eV below E_F . However, GGA+U calculations (red curves) also show curved band structure near the kink energy, which is not observed from the electronic band structure of clean graphene, but induced due to an hybridization between the adsorbate electrons and the graphene π bands. When the strength of electron-phonon coupling is determined by the slope of the dispersion below and above the kink energy, this curved band structure results in finite strength, despite the theory does not include the electron-phonon coupling. This is the so-called band structure effect [13]. In addition, nearness to the van Hove singularity is supposed to spread the measured spectral intensity away from the calculated Fermi momentum, which is beyond the capability of our first principle calculations. This spread out intensity results in the decrease of the slope near E_F and hence the apparent enhancement of electron-phonon coupling [13]. Similar band structure effects have been extensively discussed in the literature for Ca/G and K/G [12–14]. In contrast, perpendicular to the Γ K direction (Fig. 4(b)), these non-trivial effects are not observed allowing us to extract information on the electron-phonon coupling.

We now focus on the near E_F dispersion of as grown graphene and Yb/G perpendicular to the Γ K direction in Figs. 5(a) and 5(b), respectively. It is clear that, while the strength of the kink varies considerably, the characteristic energy of the kink, 0.16 eV below E_F , does not change much. This implies a stronger coupling of electrons to the optical phonon of graphene at the K point (A_{1g} mode with an energy $\hbar\omega_{ph} \approx 0.16$ eV) rather than the one at the Γ point (E_{2g} mode with an energy $\hbar\omega_{ph} \approx 0.19$ eV), in agreement with previous reports for as grown graphene [44] and as expected in the case of enhanced electronic correlations [45]. Similar conclusion can be drawn from the real part of the electron self-energy ($\text{Re}\Sigma$), i. e., the difference between the measured band and the tight-binding band, and from the imaginary part of electron self-energy ($\text{Im}\Sigma$) which is proportional to the full width at half maximum (FWHM) of

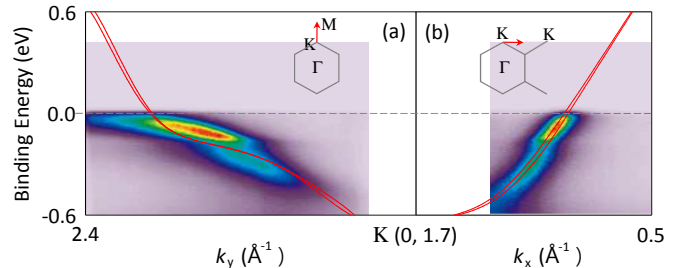


FIG. 4. (Color online) Measured and calculated Yb/G band along the KM direction (panel (a)) and perpendicular to the Γ K direction (panel (b)). The red curves are GGA+U bands.

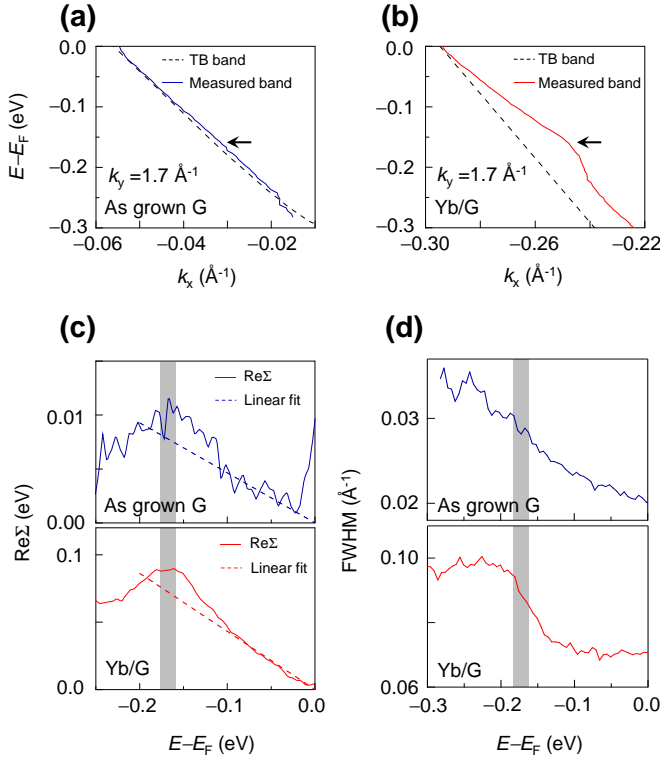


FIG. 5. (Color online) (a-b) Zoomed-in view of the electronic band structure with a kink denoted by the arrow. The dashed line is a tight-binding (TB) band fitted to each case. (c) $\text{Re}\Sigma$ for as grown G (upper panel) and Yb/G (lower panel). The dashed line is a linear fit to $\text{Re}\Sigma$ for $-0.10 \text{ eV} \leq E - E_F \leq -0.03 \text{ eV}$. Shaded area $0.16 \sim 0.18 \text{ eV}$ below E_F is a peak position of the $\text{Re}\Sigma$ spectrum. (d) MDC width as a function of $E - E_F$ for as grown G (upper panel) and Yb/G (lower panel).

MDCs. In Figs. 5(c) and 5(d), we report the $\text{Re}\Sigma$ and FWHM spectra. $\text{Re}\Sigma$, in both cases, is dominated by a strong peak at $0.16 \sim 0.18 \text{ eV}$ (gray shaded area), while the FWHM exhibits an enhanced quasiparticle scattering rate (or increased width) around the same energy. The shape of $\text{Re}\Sigma$ and $\text{Im}\Sigma$ for Yb/G is consistent with the theoretical prediction of the electron-phonon coupling for highly electron-doped graphene [46]. The upturn of the $\text{Re}\Sigma$ spectra close to E_F is a well-known resolution effect, which typically results in the deflection of MDC peaks within a few tens meV near E_F to lower momentum [47, 48], and would result in the apparent increase of $\text{Re}\Sigma$ close to E_F .

The real part of electron self-energy is a direct measurement of the electron-phonon coupling constant, given by $\lambda = |\partial \text{Re}\Sigma(E) / \partial E|_{E_F}$. The dashed line in Fig. 5(c) is a linear fit to $\text{Re}\Sigma$ for $-0.10 \text{ eV} \leq E - E_F \leq -0.03 \text{ eV}$. We obtain $\lambda = 0.046 \pm 0.002$ for as grown graphene, which is similar to the previously reported theoretical ($\lambda = 0.02$) [5] and experimental ($\lambda = 0.14$) [44] values. The difference from the latter might originate from the method to extract λ . For Yb/G, we obtain $\lambda = 0.431 \pm 0.004$, which

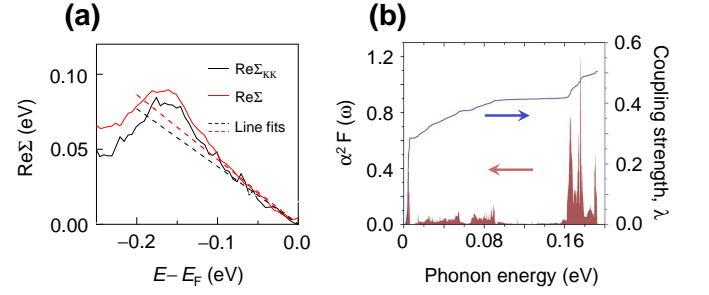


FIG. 6. (Color online) (a) $\text{Re}\Sigma$ (red line) and $\text{Re}\Sigma_{\text{KK}}$ (black line) for Yb/G. Dashed lines are linear fits to $\text{Re}\Sigma$ and $\text{Re}\Sigma_{\text{KK}}$ for $-0.10 \text{ eV} \leq E - E_F \leq -0.03 \text{ eV}$ and $-0.1 \text{ eV} \leq E - E_F \leq 0 \text{ eV}$, respectively. (b) Calculated electron-phonon coupling spectrum $\alpha^2 F(\omega)$ (brown shaded area) and the evolution of λ as a function of phonon energy (navy curve) for Yb/G.

exhibits strong enhancement by an order of magnitude compared to the value for as grown graphene. It is important to note that the GGA+U band in Fig. 3(d) does not show the decreasing slope of the dispersion near E_F , so the band structure effect is safely excluded as the origin of the enhanced λ [13]. The self-consistency of the self-energy analysis is obtained via Kramers-Kronig transformation of $\text{Im}\Sigma$ [49] as shown in Fig. 6(a). The strength of the electron-phonon coupling is obtained by linear fits to $\text{Re}\Sigma$ and $\text{Re}\Sigma_{\text{KK}}$ (brown dashed lines) for $-0.10 \text{ eV} \leq E - E_F \leq -0.03 \text{ eV}$ and $-0.1 \text{ eV} \leq E - E_F \leq 0 \text{ eV}$, resulting in $\lambda = 0.431 \pm 0.004$ and $\lambda_{\text{KK}} = 0.385 \pm 0.011$, respectively.

The calculated electron-phonon coupling spectrum and electron-phonon coupling constant for Yb/G (shown in Fig. 6(b)) are obtained from the density-functional perturbation theory using the program QUANTUM ESPRESSO [50]. The electronic orbitals were expanded in a plane-wave basis set with a kinetic energy cutoff of 75 Ry. The Brillouin zone integrations in the electronic and phonon calculations were performed using Monkhorst-Pack [51] meshes. We refer to meshes of k -points for electronic states and meshes of q -points for phonons. The electron-phonon coupling matrix elements were computed in the first Brillouin zone on a $18 \times 18 \times 1$ q -mesh using individual electron-phonon coupling matrices obtained with a $36 \times 36 \times 1$ k -points mesh. The electron-phonon coupling spectrum, $\alpha^2 F(\omega)$, (brown shaded area in Fig. 6(b)), can be divided into three regions: (i) low-energy Yb-related modes up to 0.005 eV ; (ii) carbon out-of-plane modes up to 0.09 eV ; and (iii) carbon in-plane modes at $0.16 \sim 0.18 \text{ eV}$ and 0.19 eV . We find very strong electronic coupling to the phonon mode at $0.16 \sim 0.18 \text{ eV}$ in agreement with our observation (see Fig. 5(c)). The coupling strength can be directly determined from the spectra being $\lambda = 2 \int d\omega \alpha^2 F(\omega) / \omega$ (navy curve in Fig. 6(b)). Clearly the electron-phonon coupling constant is drastically enhanced with respect to the as grown sample over the entire range, from $\lambda = 0.02$ for

as grown graphene [5] to $\lambda=0.51$ for Yb/G, consistent with the observed enhancement from $\lambda=0.05$ to $\lambda=0.43$ (Fig. 5). The difference of the experimental λ from the theoretical value might be caused by the lack of the exact unrenormalized band in extracting $\text{Re}\Sigma$, which underestimates experimental λ [9].

The observed enhancement up to 0.43 (experimental) and 0.51 (theoretical) due to Yb is far greater than the theoretically and experimentally estimated enhancement up to ~ 0.09 by the change of charge carrier density up to $n=1.7\times 10^{14}$ cm^{-2} [5, 9], as for the Yb/G sample. This indicates that charge doping alone cannot explain the observed enhancement. Similar enhancement beyond the capability of charge carrier density has been observed for potassium-intercalated graphene on Ir substrate [52, 53] with $\lambda=0.2\sim 0.28$. In the case of calcium-intercalate graphene on Au/Ni(111)/W(110) substrate [54], the anisotropic increase of λ from 0.17 (along the ΓK direction) to 0.40 (along the KM direction) has been controversial as ascribed to a change of the electron band structure and the van Hove singularity due to the Ca intercalation, which result in apparent enhancement of λ [13, 14].

The observed $\lambda=0.43$ in our work is the highest value ever measured for graphene. It is interesting to note that, for bulk graphite, the electron-phonon coupling in the Yb intercalated sample (Yb-GIC) is estimated to be weaker than that in the Ca intercalated sample (Ca-GIC), because of the slightly larger interlayer separation which leads to a decrease of the interlayer- π^* electron-phonon matrix element and thus smaller superconducting phase transition temperature, T_c (6.5 K for Yb-GIC versus 11.5 K for Ca-GIC [55]). This trend is reversed in their graphene counterparts, $\lambda=0.43$ for Yb/G (in this work) versus $\lambda=0.4$ (or 0.17) for Ca/G [54] suggesting that the hybridization between graphene π bands and the electrons from adatoms governs the low energy excitations in monolayer graphene. The hybridization induces strong Coulomb interactions, as evidenced by the preminent role of the K point phonon compared to the Γ point phonon in the electron-phonon coupling [45] as shown in Figs. 5 and 6, and allows phonons to be strongly coupled to electrons in graphene.

In line with the plausible phonon-mediated superconductivity in Yb-GIC, the strong enhancement of electron-phonon coupling in Yb/G suggests the exciting possibility that the introduction of Yb might induce superconductivity [56, 57]. The T_c is calculated using the Allen-Dynes equation [58],

$$T_c = \frac{\Omega_{log}}{1.2} \exp\left(-\frac{1.04(1+\lambda)}{\lambda - \mu^*(1+0.62\lambda)}\right). \quad (1)$$

The normalized weighting function of the Eliashberg the-

ory [56] is

$$g(\omega) = \frac{2}{\lambda\omega} \alpha^2 F(\omega). \quad (2)$$

The parameter λ is a dimensionless measure of the strength of $\alpha^2 F$ with respect to frequency ω :

$$\lambda = 2 \int_0^\omega d\omega' \alpha^2 F(\omega')/\omega', \quad (3)$$

and the logarithmic average frequency, Ω_{log} in units of K, is

$$\Omega_{log} = \exp\left(\int_0^\infty g(\omega) \ln \omega d\omega\right). \quad (4)$$

The predicted T_c and Ω_{log} are estimated to be 1.71 K and 168.2 K, respectively. We use $\mu^*=0.115$ for proper comparison with another theoretical work [8] and it is worth to note that the predicted T_c can range from 2.17 K ($\mu^*=0.10$) to 1.33 K ($\mu^*=0.13$).

V. SUMMARY

We have reported experimental evidence of strong enhancement of electron-phonon coupling in graphene by as much as a factor of 10 upon the introduction of Yb (from $0.02\leq\lambda\leq 0.05$ to $0.43\leq\lambda\leq 0.51$). Such an enhancement goes beyond what one would expect by charge doping. Our results reveal the important role of the hybridization between electrons from Yb adatoms and the graphene π electrons, pointing to such hybridization as a critical parameter in realizing correlated electron phases in graphene.

ACKNOWLEDGMENTS

The experimental part of this work was supported by Berkeley Lab's program on sp² bond materials, funded by the U.S. Department of Energy, Office of Science, Office of Basic Energy Sciences, Materials Sciences and Engineering Division, of the U.S. Department of Energy (DOE) under Contract No. DE-AC02-05CH11231. Work at the Molecular Foundry was supported by the Office of Science, Office of Basic Energy Sciences, of the U.S. Department of Energy under Contract No. DE-AC02-05CH11231. The theoretical part of this work was supported by NSF Grant No. DMR-IO-1006184 and the theory program at the Lawrence Berkeley National Laboratory through the Office of Basic Energy Science, US Department of Energy under Contract No. DE-AC02-05CH11231 (K. T. C., J. N., and M. L. C.); and by the Energy Frontier Research in Extreme Environments Center (EFree) under award number de-sg0001057. B. J. acknowledges financial support from the European Research Council (ERC-2008-AdG-No. 228074).

-
- [1] D. K. Efetov and P. Kim, Phys. Rev. Lett. **105**, 256805 (2010).
- [2] K. C. Rahnejat et al., Nature Commun. **2**, 558 (2011).
- [3] B. Uchoa and A. H. Castro Neto, Phys. Rev. Lett. **98**, 146801 (2007).
- [4] A. K. Geim and K. S. Novoselov, Nat. Mater. **6**, 183 (2007).
- [5] M. Calandra and F. Mauri, Phys. Rev. B **76**, 205411 (2007).
- [6] C. Faugeras et al., Phys. Rev. Lett. **103**, 186803 (2009).
- [7] J. C. W. Song, M. Y. Reizer, and L. S. Levitov, Phys. Rev. Lett. **109**, 106602 (2012).
- [8] G. Profeta, M. Calandra, and F. Mauri, Nat. Phys. **8**, 131 (2012).
- [9] D. A. Siegel, C. Hwang, A. V. Fedorov, and A. Lanzara, New J. Phys. **14**, 095006 (2012).
- [10] G. Savini, A. C. Ferrari, and F. Giustino, Phys. Rev. Lett. **105**, 037002 (2010).
- [11] N. W. Ashcroft and N. D. Mermin, *Solid State Physics* (Saunders College, New York, 1976).
- [12] J. L. McChesney et al., e-print, arXiv:0705.3264 (2007).
- [13] M. Calandra and F. Mauri, Phys. Rev. B **76**, 161406(R) (2007).
- [14] C. -H. Park et al., Phys. Rev. B **77**, 113410 (2008).
- [15] T. Valla et al., Phys. Rev. Lett. **102**, 107007 (2009).
- [16] S. -L. Yang et al., Nat. Commun. **5**, 2 (2014).
- [17] E. Rollings et al., J. Phys. Chem. Solids **67**, 2172 (2006).
- [18] S. Watcharinyanon, C. Virojanadara, and L. I. Johansson, Surf. Sci. **605**, 1918 (2011).
- [19] S. Watcharinyanon, L. I. Johansson, C. Xia, and C. Virojanadara, J. Vac. Sci. Technol. A **31**, 020606 (2013).
- [20] S. Watcharinyanon, L. I. Johansson, C. Xia, J. I. Flege, A. Meyer, J. Falta, and C. Virojanadara, Graphene **2**, 66 (2013).
- [21] M. L. Cohen, Phys. Scr. **T1**, 5 (1982).
- [22] G. Kresse and J. Hafner, Phys. Rev. B **47**, 558 (1993).
- [23] G. Kresse and J. Furthmüller, Computational Materials Science **6**, 15 (1996).
- [24] G. Kresse and J. Furthmüller, Phys. Rev. B **54**, 11169 (1996).
- [25] P. E. Blöchl, Phys. Rev. B **50**, 17953 (1994).
- [26] G. Kresse and D. Joubert, Phys. Rev. B **59**, 1758 (1999).
- [27] J. P. Perdew, K. Burke, and M. Ernzerhof, Phys. Rev. Lett. **77**, 3865 (1996).
- [28] A. I. Liechtenstein, V. I. Anisimov, and J. Zaanen, Phys. Rev. B **52**, R5467 (1995).
- [29] I. I. Mazin and S. L. Molodtsov, Phys. Rev. B **72**, 172504 (2005).
- [30] C. Hwang et al., Phys. Rev. B **84**, 125422 (2011).
- [31] D. A. Siegel et al., Appl. Phys. Lett. **93**, 243119 (2008).
- [32] A. Grüneis et al., Phys. Rev. B **78**, 205425 (2008).
- [33] S. Y. Zhou et al., Nat. Mater. **6**, 770 (2007).
- [34] S. Kim et al., Phys. Rev. Lett. **100**, 176802 (2008).
- [35] E. Rotenberg et al., Nat. Mater. **7**, 258 (2008).
- [36] S. Y. Zhou et al., Nat. Mater. **7**, 259 (2008).
- [37] A. Bostwick et al., Science **328**, 999 (2010).
- [38] J. Lischner, D. Vigil-Fowler, and S. G. Louie, Phys. Rev. Lett. **110**, 146801 (2013).
- [39] S. Verga, A. Knigavko, and F. Marsiglio, Phys. Rev. B **67**, 054503 (2003).
- [40] F. Reinert and S. Hüfner, New J. Phys. **7**, 97 (2005).
- [41] M. Hengsberger et al., Phys. Rev. B **60**, 10796 (1999).
- [42] A. Lanzara et al., Nature **412**, 510 (2001).
- [43] G. -H. Gweon et al., Nature **430**, 187 (2004).
- [44] S. Y. Zhou, D. A. Siegel, A. V. Fedorov, and A. Lanzara, Phys. Rev. B **78**, 193404 (2008).
- [45] D. M. Basko and I. L. Aleiner, I. L. Phys. Rev. B **77**, 041409(R) (2008), (and references therein).
- [46] C. -H. Park, F. Giustino, M. L. Cohen, and S. G. Louie, Phys. Rev. Lett. **99**, 086804 (2007).
- [47] N. C. Plumb et al., Phys. Rev. Lett. **105**, 046402 (2010).
- [48] T. Valla, Phys. Rev. Lett. **96**, 119701 (2006).
- [49] A.A. Kordyuk, S.V. Borisenko, A. Koitzsch, J. Fink, M. Knupfer, and H. Berger, Phys. Rev. B **71**, 214513 (2005).
- [50] S. Baroni, S. de Gironcoli, A. Dal Corso, and P. Gianozzi, Rev. Mod. Phys. **73**, 515 (2001).
- [51] H. J. Monkhorst and J. D. Pack, Phys. Rev. B **13**, 51882 (1976).
- [52] M. Bianchi et al., Phys. Rev. B **81**, 041403(R) (2010).
- [53] I. Pletikosić, M. Kralj, M. Milum, and P. Pervan, Phys. Rev. B **85**, 155447 (2012).
- [54] A. V. Fedorov et al., Nat. Commun. **5**, 3257 (2014).
- [55] T. E. Weller et al., Nat. Phys. **1**, 39 (2005).
- [56] W. L. McMillan, Phys. Rev. **167**, 331 (1968).
- [57] A. C. Rose-Innes and E. H. Rhoderick, *Introduction to Superconductivity* (Pergamon Press, 1978).
- [58] P. B. Allen and R. C. Dynes, Phys. Rev. B **12**, 905 (1975).